

Study of Laminated Veneer Lumber (LVL) Sengon to Concrete Joint Using Two-Dimensional Numerical Simulation

Urwatul Wusqo, Ali Awaludin*, Inggar Septhia Irawati, Angga Fajar Setiawan

Civil and Environmental Engineering Department, Universitas Gadjah Mada, INDONESIA

*Corresponding authors: ali.awaludin@ugm.ac.id

SUBMITTED 16 July 2019 REVISED 31 July 2019 ACCEPTED 16 August 2019

ABSTRACT The connection system is a critical part of Timber – Concrete Composite (TCC) floor structures. The behaviour of the connection needs to be known to predict the behaviour of composite structure accurately. Screws are one kind of connector that mostly used in the composite structure due to its installation ease and high withdrawal strength. This study carried out a two-dimensional numerical simulation to examine the behaviour of LVL Sengon-concrete joint using OpenSees software. The lag screw used to connect LVL Sengon and concrete. In this simulation, the screw was assumed as a beam with hinges element that supported by a set of springs representing the strength of LVL Sengon and concrete. Some input parameters for this simulation were obtained from the material test and previous research. The effect of secondary axial force was considered into the load-displacement curve resulted from the numerical simulation. This study performed several simulations towards the variation of the screw diameter, penetration depth, and concrete compressive strength. The capacity of the connections resulted from the numerical simulation were overestimates the manual calculation using EYM theory and NDS 2018 equations. The capacity of the connection increased about 146% to 284% due to the addition of secondary axial forces. In addition, this simulation can adequately predict the shear force, bending moment, and deformation of the screw. There is a plastic hinge formed in the screw after the screw being deformed a quite large. It shows the same yield mode with the manual calculation using EYM theory and NDS 2018 equations. This simulation also can show the contribution of each spring elements to resist the load until its ultimate strength.

KEYWORDS LVL Sengon; Secondary axial force; Timber to the concrete joint; Numerical simulation; Opensees

© The Author(s) 2019. This article is distributed under a Creative Commons Attribution-ShareAlike 4.0 International license.

1 INTRODUCTION

Laminated Veneer Lumber (LVL) is an engineering wood that is made by gluing layers of timber with 2.5 mm to 4.8 mm thickness using adhesive. Some veneers of timber are arranged in the vertical or horizontal direction to form a laminated beam and cut into the required dimension. The beam that composed by vertically arranged veneers has higher strength although its stiffness is lower (Tjondro, et al., 2011). LVL Sengon is one of engineering wood that currently available in Indonesia. Compared to Sengon solid timber, LVL Sengon has better mechanical properties, as shown in Table 1.

A composite structure is a kind of structure obtained by combining two or more materials that aim to get a structure with better performance. In the LVL -Concrete composite floor, the composite action between LVL and timber

can reach 95% if the connection system between LVL and concrete designed properly (Yeoh, et al., 2011). Design of the shear connector in a composite structure is related to not only the number of connectors being installed in the composite structure but also the behaviour of the shear connector itself. The response of the TCC floor structure can be predicted accurately if the behavior of the shear connector is considered (Oudjene, et al., 2018).

Manual calculation using *European Yield Model (EYM)* theory and *National Design Specification (NDS) 2018* can predict the load-carrying capacity of the connection without knowing the behaviour of the connection. The behavior of the connection can be predicted using numerical simulation or experimental test.

Table 1. Mechanical properties of Sengon solid and LVL Sengon (Awaludin, et al., 2018)

Mechanical properties	Sengon solid	LVL Sengon
Density	0.26	0.41
MOE (N/mm ²)	1250-3300	5700-9000
MOR (N/mm ²)	30	39-40.57
Compression// (N/mm ²)	2.09	4.03
Compression ⊥ (N/mm ²)	3.52	5.40
Tension //(N/mm ²)	20.00	46.69

Numerical simulation is often chosen due to its easiness and practicality. Meghlat et al. (2013) modeled screwed timber joint using ABAQUS software in which they used a one-dimensional beam element to represent the steel screws and solid element for the timber. This simulation can predict the load-slip curve of the connection accurately in the elastic zone. Oudjene, et al. (2013) proposed a numerical model of screwed timber to concrete joint in detailed 3D finite element model and could accurately predict the nonlinear behaviour of the connection until a slip level of 20 mm.

Izzi et al. (2016) had performed a numerical simulation to simulate steel to timber joints for CLT structure.

The fastener shank was simulated using non-linear beam element that interconnected with hinges. The result shows that the simulation can be implemented in a general model of the connection to predict the behavior of the connection after being compared by the experimental work. Hassanieh et al. (2017) had carried out a validation of three-dimensional finite element model of LVL to steel connection using bolt and coach screw and found that the friction force between steel and LVL affect the peak load capacity of the connection with screw connection. Numerical simulation using three-dimensional model sometimes is complicated and needs high specification hardware. Therefore, this study performed a numerical simulation in the two-dimensional model to obtain a new approach of connection model to predict the behavior of the LVL Sengon to concrete joint using a screw as its fastener. This simulation also considered The effect of the secondary axial force on the load-carrying capacity of the joints.

2 METHODS

2.1 Methodology

Figure 1 shows the study methodology.

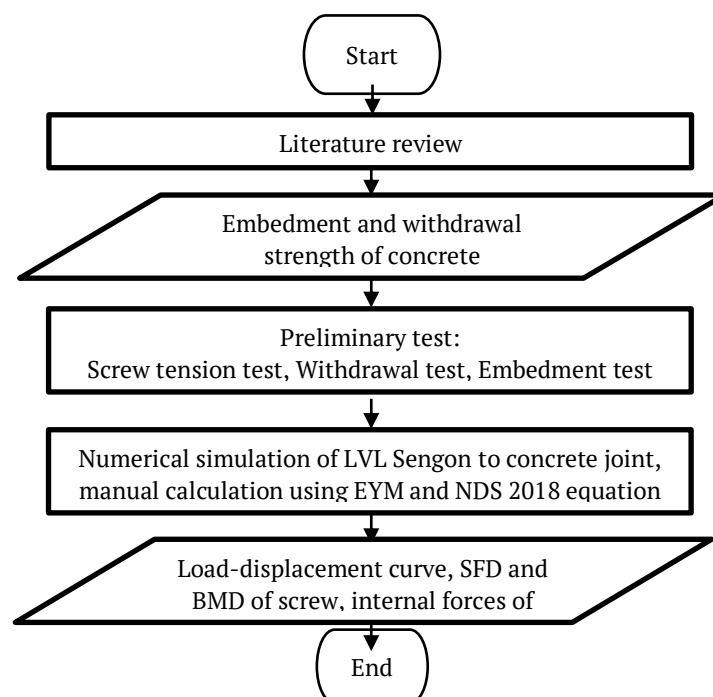


Figure 1. Flow diagram of the methodology

2.2 Preliminary test

Some preliminary test was performed, to obtain the material behaviour as an input parameter for the numerical simulation. According to ASTM E8M, the tensile test provides information on the strength and ductility of the materials under uniaxial tensile stress and shown in Figure 2.(a). From the result of the screw tensile test shown in Figure 2.(b), steel as the screw material behaves as bilinear material.

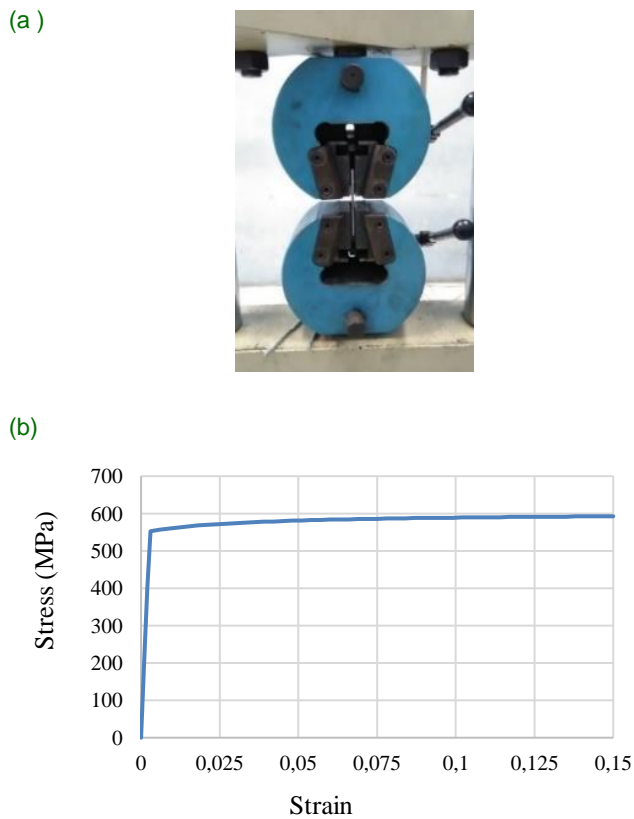


Figure 2. (a) Screw tensile test, (b) Stress-strain relationship of steel

The specimen for embedment test consists of 40 mm x 80 mm x 60 mm of LVL Sengon and screw with a diameter of 8 mm and 6 mm. A screw was placed on top of LVL Sengon, and the force was applied over the screw through a loading plate, as shown in Figure 3.(a). Figure 3.(b) and 3.(c) show that the behaviour of the embedment strength of LVL Sengon corresponds to elasto-perfectly plastic material.

Screw withdrawal test was performed based on ASTM D1037 to evaluate the resistance of LVL Sengon due to screw withdrawal.

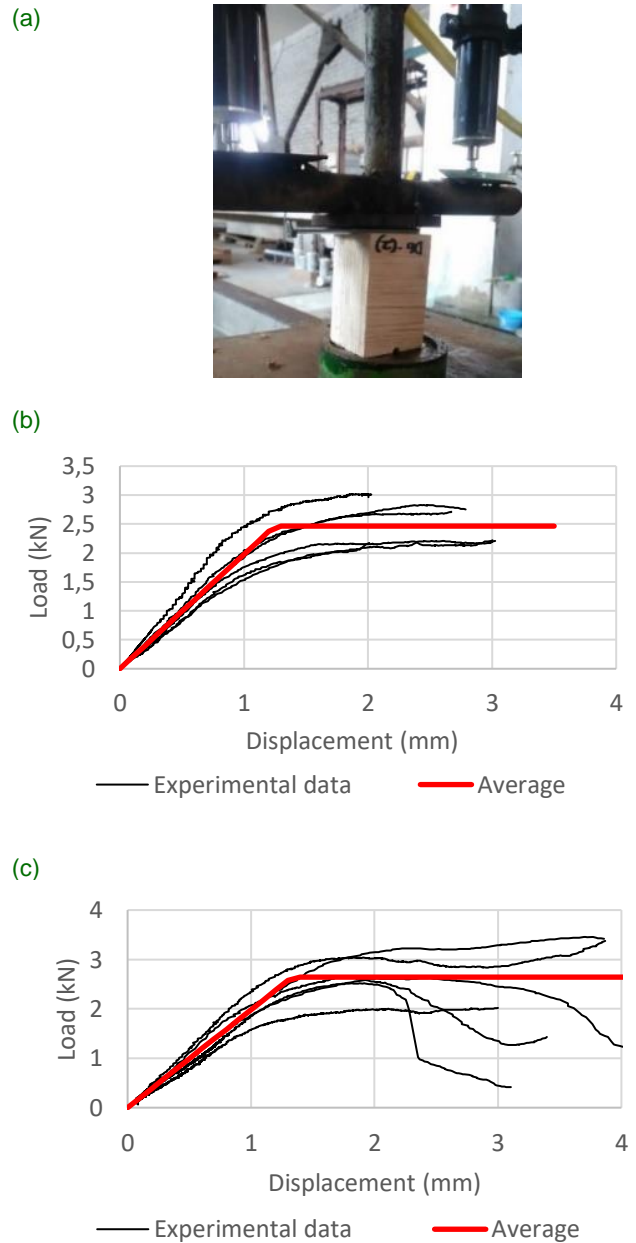


Figure 3. (a) Embedment test, (b) Load-displacement curve for a screw with a diameter of 6mm, and (c) Load-displacement curve for screw with a diameter of 8mm.

Six specimens consist of 40 mm x 80 mm x 200 mm LVL Sengon and screw with diameter 8 mm and 6 mm. Force is applied to the screw, as shown in Figure 4.(a).

Figure 4.(b) and 4.(c) show that the withdrawal strength behaves as bilinear material. The withdrawal strength of LVL Sengon increased until reaching its maximum strength, then run into the softening stage along with the increase of slip.

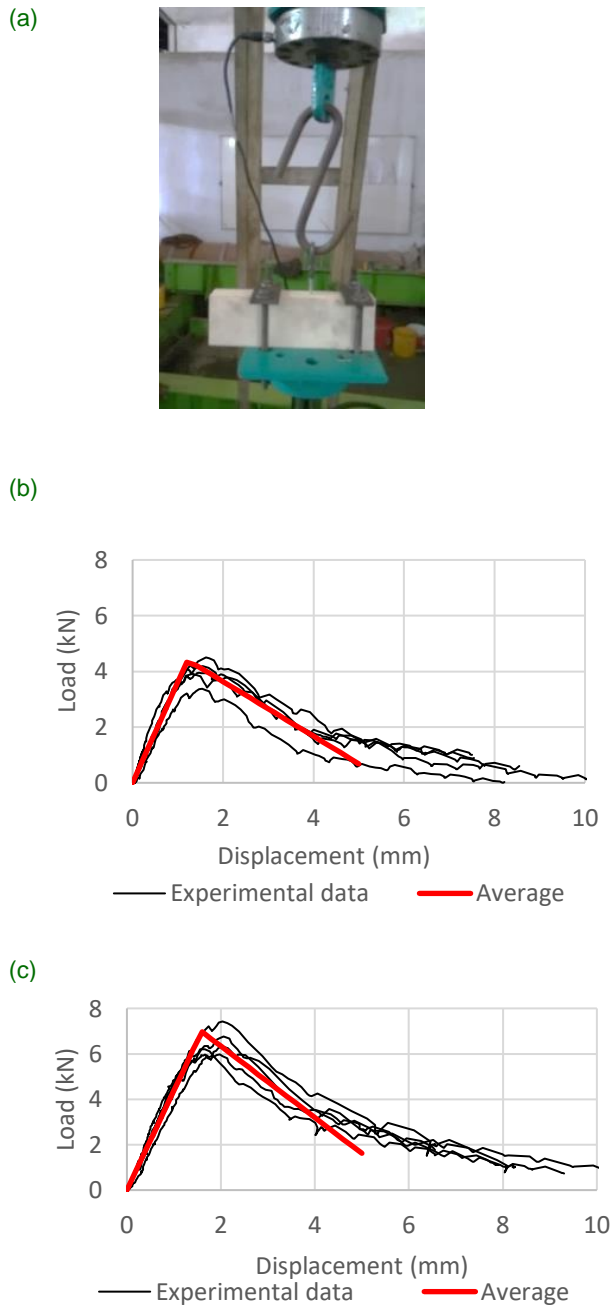


Figure 4. (a) Withdrawal test, (b) Load-displacement curve for a screw with a diameter of 6mm, and (c) Load-displacement curve for a screw with a diameter of 8mm.

2.3 The Load Carrying Capacity of the Connection

European Yield Model (EYM) theory and National Design Specification (NDS) 2018 are the popular theory to calculate the load-carrying capacity of the connection.

Both EYM and NDS 2018 can predict the load-carrying capacity of the connection in some yield mode only, as shown in Figure 5. *European Yield Model* (EYM) that was proposed by Johansen in 1949 assumed that the embedment strength of wood and fastener bending strength behaves as rigid plastic material. The connection achieves its load-carrying capacity when the embedment strength of the connected member under the screw reaches its ultimate strength, or there is a formation of one or more plastic hinge in the screw followed by the occurrence of plastic stress in the timber element. According to EYM theory, the load-carrying capacity of a screw (Z) can be determined using Equation 1 to 4 (Awaludin, 2005). A connection that uses nails, screws, dowels, and bolts belongs to metal dowel type connection. Metal dowel connection is a ductile connection even though it has a lower load-carrying capacity compared by notch and plate connection (Dias, et al., 2015).

$$Z(I_s) = \frac{3.3 D t_s F_{es}}{K_D} \tag{1}$$

$$Z(III_m) = \frac{3.3 k_1 D p F_{em}}{K_D (1+2 R_e)} \tag{2}$$

$$Z(III_s) = \frac{3.3 k_2 D t_s F_{em}}{K_D (2+R_e)} \tag{3}$$

$$Z(IV) = \frac{3.3 D^2}{K_D} \sqrt{\frac{2 F_{em} F_{yb}}{3 (1+R_e)}} \tag{4}$$

In Equation 1 to 4, t_m is the thickness of the main timber member, t_s is the thickness of the side member, D is the fastener diameter, p is the depth of the fastener penetration, and K_D is the reduction factor. F_{em} and F_{es} is the embedment strength of the main and side member, respectively. R_e is the ratio between F_{em} and F_{es} . The value of k_1 and k_2 in Equation 3 to 6 must be determined using Equation 5 and 6 (Awaludin, 2005).

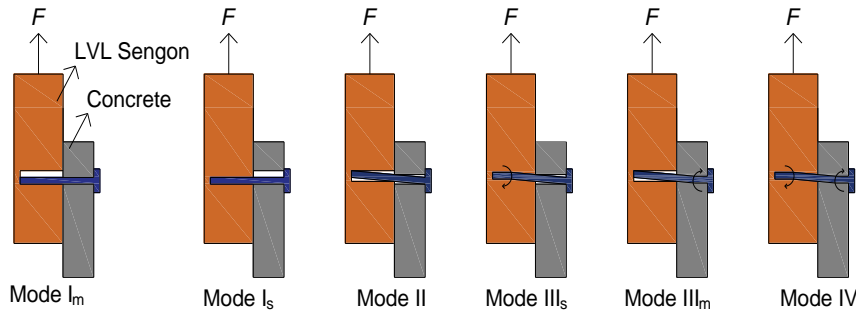


Figure 5. Yield mode in single shear connection

$$k_1 = (-1) + \sqrt{2(1 + R_e) + \frac{2F_{yb}(1+2R_e)D^2}{3F_{em}p^2}} \quad (5)$$

$$k_2 = (-1) + \sqrt{\frac{2(1 + R_e)}{R_e} + \frac{2F_{yb}(1+2R_e)D^2}{3F_{em}t_s^2}} \quad (6)$$

National Design Specification (NDS) 2018 also provides several equations for calculating the load-carrying capacity of wood-based connection (Z) in several yield modes, as shown in Equation 7 to 12.

$$Z(I_m) = \frac{D\ell_m F_{em}}{R_d} \quad (7)$$

$$Z(I_s) = \frac{D\ell_s F_{es}}{R_d} \quad (8)$$

$$Z(II) = \frac{k_1 D\ell_s F_{es}}{R_d} \quad (9)$$

$$Z(III_m) = \frac{k_3 D\ell_s F_{em}}{(1+2R_e)R_d} \quad (10)$$

$$Z(III_s) = \frac{k_3 D\ell_s F_{em}}{(2+R_e)R_d} \quad (11)$$

$$Z(IV) = \frac{D^2}{R_d} \sqrt{\frac{2F_{em}F_{yb}}{3(1+R_e)}} \quad (12)$$

In Equation 7 to 12, ℓ_m is the embedment length of the fastener in the main timber member, ℓ_s is the embedment length of the fastener in the side member, and R_D is the reduction factor. R_t is the ratio between ℓ_m and ℓ_s .

According to NDS 2018, the value of $k_1, k_2,$ and k_3 in Equation 7 to 12 must be determined using Equation 13 to 15.

$$k_1 = \frac{\sqrt{R_e + R_e^2(1+R_t+R_t^2) + R_t^2 + R_e^2 - R_e(1+R_t)}}{(1+R_e)} \quad (13)$$

$$k_2 = -1 + \sqrt{2(1 + R_e) + \frac{2F_{yb}(1+2R_e)D^2}{3F_{em}\ell_m^2}} \quad (14)$$

$$k_3 = -1 + \sqrt{\frac{2(1+R_e)}{R_e} + \frac{2F_{yb}(2+R_e)D^2}{3F_{em}\ell_s^2}} \quad (15)$$

The three main parameters influencing the load-carrying capacity of joints with dowel-type fasteners is the bending capacity of the dowel, the embedding capacity, and the screw withdrawal strength. Besides that, the friction force between the connected member also influenced the load-carrying capacity of the connection.

The friction effect on the connection could arise in the failure modes that involve yielding of the fasteners, as shown in Figure 2. In addition to being subjected to bending, the fastener is also subjected to a tension force or axial force. This axial force has vertical and horizontal force components. If the axial force is N_d and rotation angle of the screw is θ , the vertical component can be written as $N_d \sin\theta$. If the friction coefficient between concrete and timber is μ , the horizontal component $N_d \cos\theta$ must be multiplied by μ to get a normal force that also acts in the vertical direction.

The presence of $N_d \sin\theta$ and $\mu N_d \cos\theta$ in the connection force gives additional resistance to the connection. Table 2 presents the value of μ for wood and concrete.

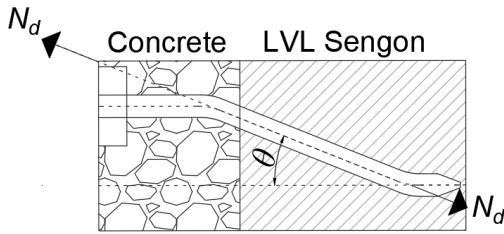


Figure 6. Secondary axial force in connection (Porteous & Kermani, 2007, with modification)

Table 2. Concrete to timber friction coefficient (Gorst, et al., 2003)

Source	μ
BS 5795 : 1996	0.4
Gorst, et al (2003)	0.7
DIN 4421 and prEN 12812	0.8

2.4 Numerical Simulation of LVL Sengon to concrete joint

Numerical simulation of LVL Sengon to concrete joint was performed using OpenSees v.2.5 finite element software. The schematization of the finite element model shown in Figure 7.

As shown in Figure 7, the fastener shank was assumed as a beam with hinges element with fibre section, with the length of each segment is 5 mm. A fibre section is a solid cross-section that consists of some fibre as described in Figure 8.

According to Du, Sun, & Xu, (2012), the use of fibre section in the analysis gives some advantages. The fibre section can include the coupling of axial force and bending moment during the analysis. A set of spring given along the screw shank supported the beam element, representing the embedment strength (red and orange springs in Figure 7) and withdrawal strength (blue and green springs in Figure 7) of LVL Sengon and concrete. The input parameter of LVL Sengon was obtained from the preliminary test, while the parameter of concrete adopted from the previous study performed by Suriani (2012) and Rao & Arora (2013). The spring element was built using two node-link elements that connect two nodes, one in the beam with hinges element and one in the rigid element located in the top and bottom of the screw. The rigid element in the LVL Sengon and the concrete side supported by roller and fixed support, respectively.

The load is applied gradually in the rigid element located in the LVL Sengon using displacement control integrator. The applied displacement increment is dU in static condition. The value of displacement increment set to the 0.001mm with the control point is at the end of the screw that located in the LVL Sengon side, as shown in Figure 9.

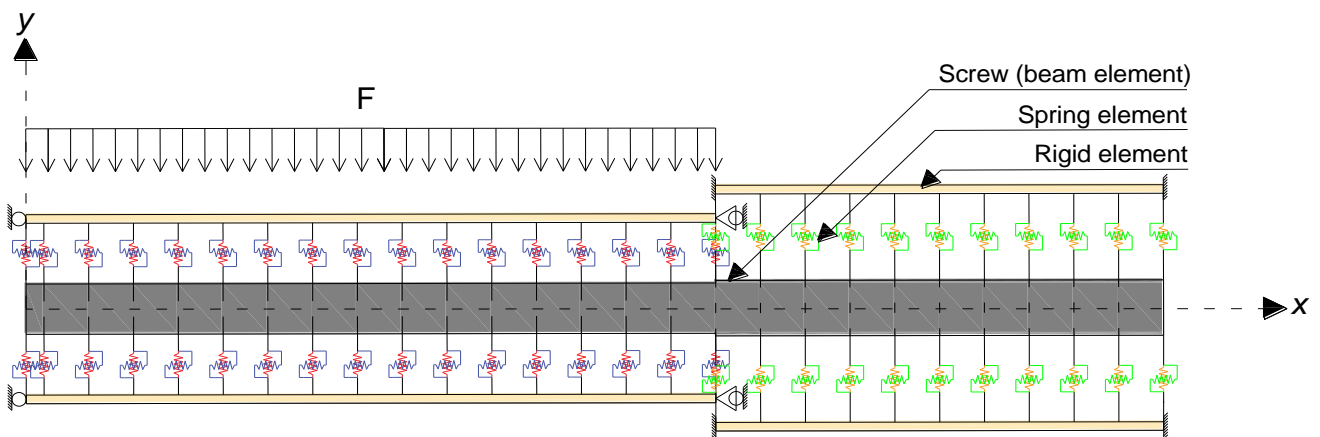


Figure 7. Finite element model of connection

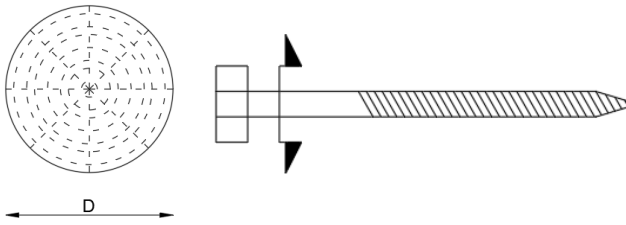


Figure 8. Fibre section

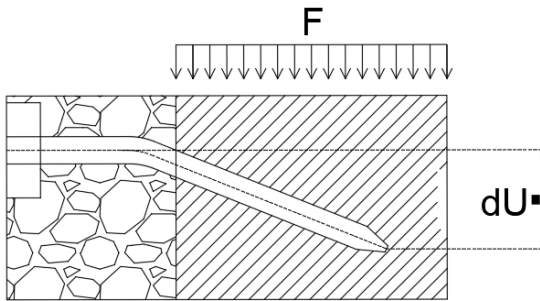


Figure 9. Loading scheme of connection

The structure is in equilibrium condition when the external work equal to the internal work. The external virtual work, W_i , is equivalent to the first variation of potential energy due to external load caused by displacement variation as described in Equation 16. The internal virtual work written in Equation 17 is the variation of strain energy, $\Lambda^{(e)}$. Equation 18 expressed the total potential energy, Π , for a structure with n elements and m nodes.

$$W_i = F_i u_i \tag{16}$$

$$\Lambda^{(e)} = \int \frac{1}{2} \sigma \varepsilon dV = \int \frac{1}{2} E \varepsilon^2 dV \tag{17}$$

$$\Pi = \sum_{e=1}^n \Lambda^{(e)} - \sum_{i=1}^m W_i = \sum_{e=1}^n \Lambda^{(e)} - \sum_{i=1}^m F_i u_i \tag{18}$$

In Equation 16 to 18, F is the external forces, and the value of u is referring to the nodal displacement. V is the volume of the system, E is the modulus of elasticity, and ε is the strain of each element. To obtain the equilibrium of the structure, Equation 18 then derived as Equation 19 and must be equal to zero. Newton Raphson and Modified Newton algorithms were used to solving Equation 19. This study performed some numerical simulation based on the availability of data and tabulated in Table 3

$$\frac{\partial \Pi}{\partial u_i} = \frac{\partial}{\partial u_i} \sum_{e=1}^n \Lambda^{(e)} - \frac{\partial}{\partial u_i} \sum_{i=1}^m F_i u_i = 0 \tag{19}$$

3 RESULTS AND DISCUSSIONS

3.1 The Load Carrying Capacity of The Connection

The load-carrying capacity of the connection can be taken from the smallest values calculated using Equations 1 to 4 (according to EYM) and Equations 7 to 12 (according to NDS 2018). The load-displacement curves resulted from the numerical simulation are then compared by the results from the theoretical calculation, shown in Figure 10.

Figure 10 shows that the connection behaves in a ductile manner. In general, the load-carrying capacity resulted from the numerical simulation is higher than EYM and NDS 2018 due to the difference assumption between theoretical calculation and numerical simulation. The numerical simulation had considered the withdrawal strength of LVL Sengon and concrete.

Table 3. Various type of numerical simulation performed

Connection Type	Concrete compressive strength (MPa)	Screw diameter (mm)	Screw length (mm)
A6x	15	6	101.6
A8x	15	8	101.6
A8y	15	8	127
B6x	20	6	101.6
B8x	20	8	101.6
B8y	20	8	127

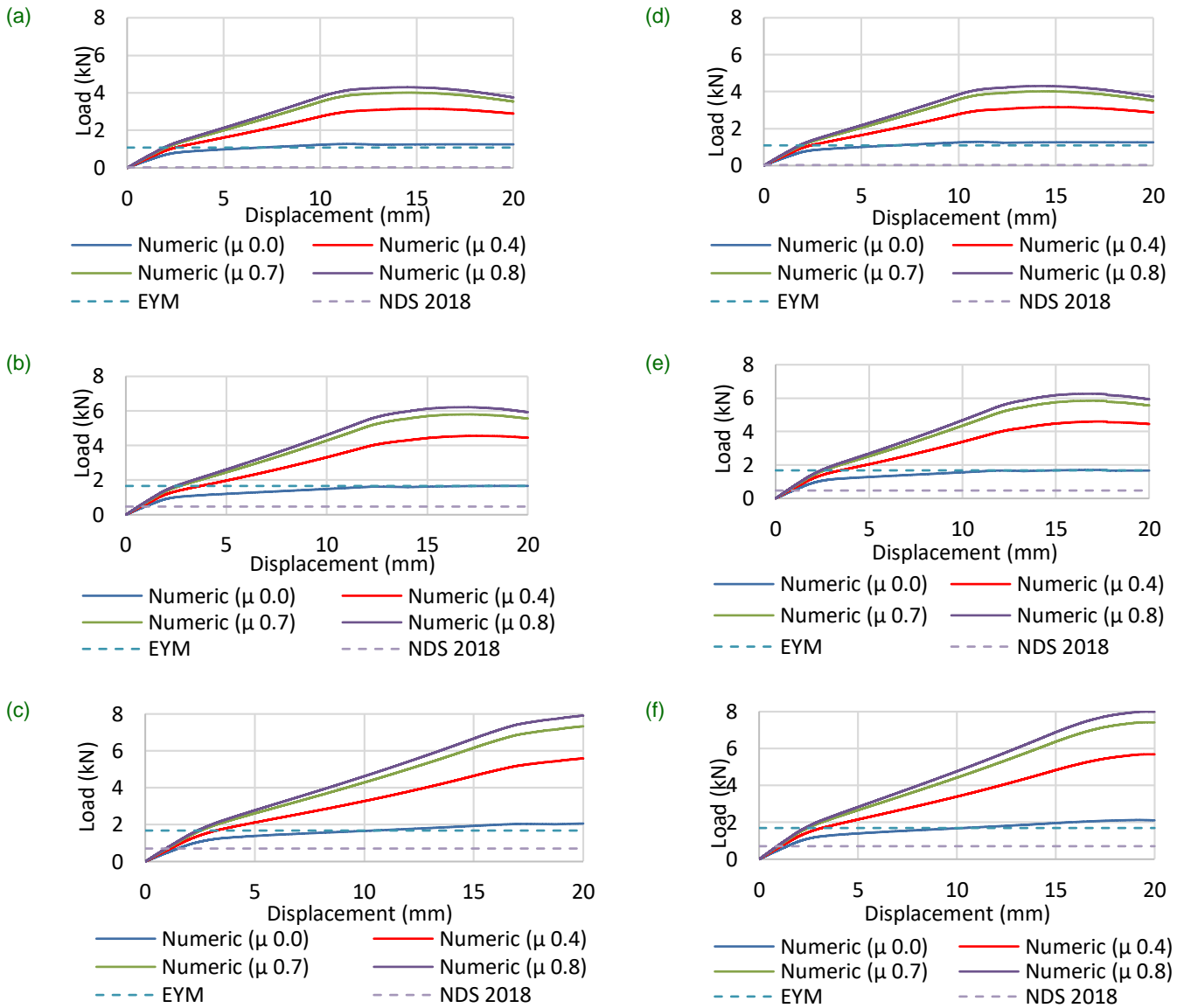


Figure 10. The load-displacement curve for several types of connections: (a). A6x, (b). A8x, (c). A8y, (d). B6x, (e). B8x, (f). B8y

As shown in Table 4, the difference of the connection capacity between numerical simulation and EYM theory varies from 0% to 26%. The difference of the connection capacity between numerical simulation and NDS 2018 varies from 192% to 4160% and caused by the great reduction factor given in NDS 2018 equation particularly when the fastener diameter is smaller than 6.35mm. Table 4 shows that the screw diameter and screw penetration depth provides a significant effect on the load-carrying capacity of the connection.

The concrete compressive strength has a minimal effect on the load-carrying capacity of the connection.

Equations in NDS 2018 and EYM equations have not considered the effect of secondary axial force yet. Meanwhile, the numerical simulation had considered the secondary axial force. Table 5 shows the effect of the secondary axial force on the connection. There is an increase of connection capacity between 146% to 284% due to the addition of secondary axial force.

Table 4. The load carrying capacity of the connection from numerical simulation and theoretical calculation

Connection type	Numerical simulation (kN)	EYM		NDS 2012	
		Capacity (kN)	Difference (%)	Capacity (kN)	Difference (%)
A6x	1.281	1.084	18	0.030	4160
A8x	1.665	1.662	0	0.472	253
A8y	2.057	1.678	23	0.704	192
B6x	1.286	1.093	18	0.030	4141
B8x	1.705	1.676	2	0.472	261
B8y	2.126	1.690	26	0.705	202

Table 5. The effect secondary axial force to the load-carrying capacity of the connection

Connection type	$\mu=0.0$	$\mu=0.4$	$\mu=0.7$		$\mu=0.8$		
	Capacity (kN)	Capacity (kN)	Increase (%)	Capacity (kN)	Increase (%)	Capacity (kN)	Increase (%)
A6x	1.281	3.154	146	4.104	213	4.301	236
A8x	1.665	4.557	173	5.799	248	6.213	273
A8y	2.057	5.585	171	7.321	255	7.899	284
B6x	1.286	3.161	146	4.021	212	4.308	235
B8x	1.705	4.600	170	5.842	242	6.256	267
B8y	2.126	5.679	167	7.410	249	7.987	276

3.2 Screw Deformation

Figure 11 shows the deformation along the screw. At the end of the loading steps, the screw formed a plastic hinge (indicated by the blue circle in Figure 11). The value of Δ in Figure 11 shows the displacement at the end of the screw (point 0,0 in Figure 11). Table 6 shows the yield mode of the connection that calculated using existing theory (EYM and NDS 2018).

The calculation results of both using EYM and NDS 2018 equations lead to failure, where the main member of the connection (LVL Sengon) failed first, and followed by a formation of a plastic hinge in the screw. According to Megson (2014), when the bending moment exceeds the yield moment of the section, M_y , and approaches the plastic moment of the screw section, M_p , unrestricted plastic flow occurred, and it leads to the formation of plastic hinges.

Table 6. Yield mode of the connection

Connection Type	Yield mode (Theoretical calculation)		Yield mode (Simulation)
	EYM	NDS 2012	Number of plastic hinges
A6x	III _m	III _m	1
A8x	III _m	I _m	1
A8y	III _m	III _m	1
B6x	III _m	III _m	1
B8x	III _m	I _m	1
B8y	III _m	III _m	1

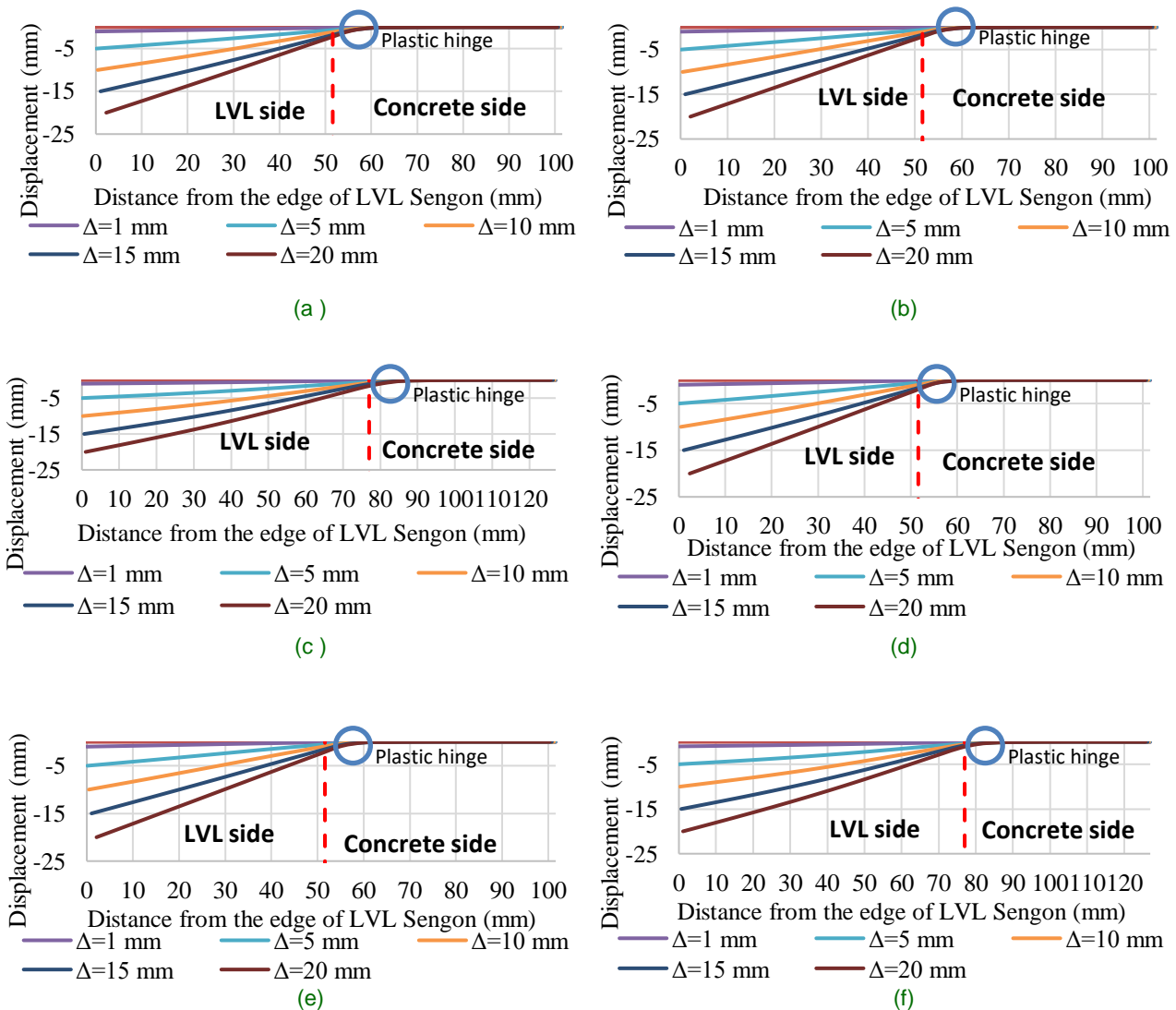


Figure 11. Screw deformation for several types of connections: (a).A6x, (b).A8x, (c).A8y, (d).B6x, (e).B8x, (f).B8y

3.3 Internal Forces of Screw

The numerical simulation results of the behavior of LVL Sengon to concrete joint show similar behavior. Figure 12 shows the shear force and bending moment distribution along the screw for B8y connection. The value of Δ in Figure 12 shows the displacement at the end of the screw (point 0,0 in Figure 12). The maximum shear force occurred near the shear plane of LVL Sengon and concrete. In this area, the screw surface changed from threaded to the smooth surface, and the diameter is also changed. Besides that, the stiffness of the spring that

supports the screw also changed. It causes stress which indicated by the maximum shear force. The great support from concrete embedment and withdrawal strength makes the screw embedded in the concrete side clamped. The moment distribution shows that the screw behaves like a cantilever beam. Figure 12.(b) shows one of the maximum bending moment value has exceeded the yield moment of the screw and has a slightly different from the plastic moment of the screw, which indicates the formation of a plastic moment on the screw. The value of the bending moment for several types of connection given in Table 7.

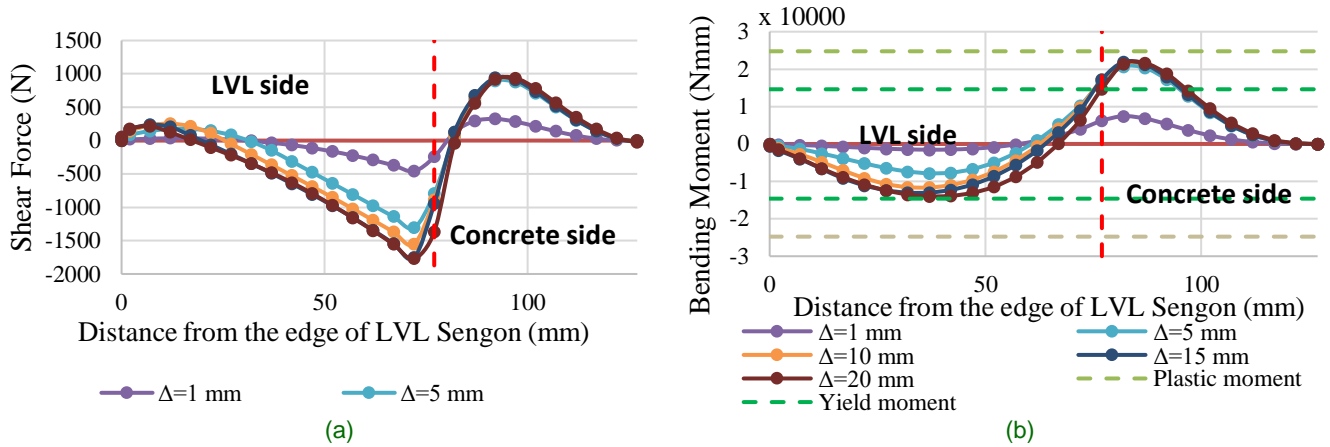


Figure 12. Screw internal forces for B8y connection: (a). Shear force diagram, (b). Bending moment diagram

Table 7. The maximum bending moment on the screw

Connection Type	Yield moment (Nmm)	Plastic moment (Nmm)	Peak 1		Peak 2	
			Bending moment (Nmm)	Yield/Not Yield	Bending moment (Nmm)	Yield/Not Yield
A6x	7879.892	13356.017	-6648.621	Not Yield	10708.465	Yield
A8x	14612.318	24767.272	-6016.334	Not Yield	16687.764	Yield
A8y	14612.318	24767.272	-15329.429	Yield	22002.422	Yield
B6x	7879.892	13356.017	-6641.026	Not Yield	10914.255	Yield
B8x	14612.318	24767.272	-5316.454	Not Yield	19142.401	Yield
B8y	14612.318	24767.272	-13990.375	Not Yield	22139.078	Yield

3.4 Internal Forces of Springs Elements

In general, the numerical simulation results regarding the behavior of LVL Sengon to concrete joint show similar behavior. Therefore, Figure 13 shows the internal forces of the spring elements for B8y connection only. The value of Δ in Figure 13 shows the displacement at the end of the screw (point 0,0 in Figure 13).

In this simulation, the embedment strength of LVL Sengon assumed as spring elements that only resist compression stress, while the embedment strength of concrete assumed as spring elements that can resist both compression and tension stress. During the loading process, lateral loads applied through LVL Sengon cause the spring elements above the screw in the LVL Sengon side experienced to compression stress.

The spring elements located over the screw experienced compression stress until it reaches the plastic limit of LVL Sengon, whereas the spring elements under the screw in the LVL

Sengon side doesn't resist any forces except the spring near the edge of LVL Sengon. It shows that the numerical simulation is suitable with the theory in which the load-carrying capacity of the connection achieved when the embedment strength of the connected member under the screw reaches its ultimate strength, or there is a formation of one or more plastic hinges in the screw followed by the occurrence of plastic stress in the timber element. The different behavior is shown by the spring elements that represent the withdrawal and embedment strength of concrete.

The spring elements both above and under the screw are resisting the load together. When the upper spring run into the compression stress, the bottom spring experienced tension stress, and it goes the other way around. Figure 13 shows that the tension stress occurred in the spring element reaches the concrete tensile strength, but the compression stress occurred in the spring element reaches the concrete tensile strength.

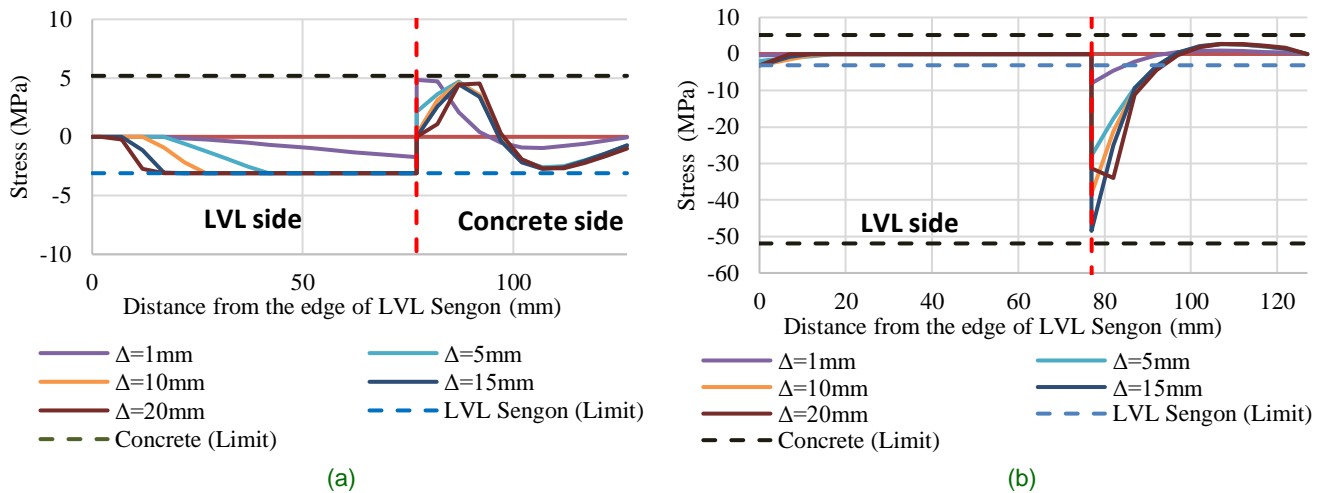


Figure 13. Internal forces of spring elements for B8y connection: (a). Springs above the screw, (b). Springs under the screw

4 CONCLUSIONS

This study performed a two-dimensional numerical simulation of LVL Sengon to concrete joint. The screw was assumed as a beam with hinges element that supported by a set of spring. Some variations of the numerical simulation were performed and resulted as follows.

- The connection capacity resulted from the numerical simulation is higher than the theoretical calculation. The difference in the connection capacity resulted from numerical simulation and EYM theory varies from 0% to 26%. The difference in the connection capacity between the result from numerical simulation and NDS 2018 Equation varies from 192% to 4160%.
- The secondary axial force gives a more load-carrying capacity of the connection about 146% to 284%.
- The maximum shear force and bending moment occurred near the shear plane of LVL Sengon and concrete. A plastic hinge formed in the maximum bending moment point which led to the same yield mode predicted by EYM theory and NDS 2018 equation in general.
- The load-carrying capacity of the connection is achieved when the embedment strength of the LVL Sengon reaches its plastic limit. From the simulation, the embedment spring

of LVL Sengon reaches its plastic deformation after the screw deforms a quite large. The embedment spring of the concrete also reaches its tension strength limit, but not its compressive strength limit.

DISCLAIMER

The authors declare no conflict of interest.

REFERENCES

- ASTM, 1999. *ASTM D1037-Standard Test Methods for Evaluating Properties of Wood-Base Fiber and Particle Panel Materials*. West Conshohocken: American Society of Testing and Material.
- ASTM, 2013. *ASTM E8M Standard Test Methods of Tension Testing of Metallic Materials*. West Conshohocken: American Society of Testing and Material.
- Awaludin, A., 2005. *Dasar-dasar Perencanaan Sambungan Kayu*. Yogyakarta: Biro Penerbit Keluarga Mahasiswa Teknik Sipil UGM. (In Indonesia)
- Awaludin, A. et al., 2018. Laminated Veneer Lumber (LVL) Sengon : An Innovative Sustainable Building Material in Indonesia. *International Journal of Integrated Engineering* , 10(1), pp. 17-22.

- AWC, 2017. *National Design Specification for Wood Construction*. 2018 ed. Leesburg: American Wood Council.
- D.Yeoh, M. Fragiaco, B.Deam, 2011. Experimental Behaviour of LVL-Concrete Composite Floor Beams at Strength Limit State. *Engineering Structure*, Volume 33, pp. 2697-2707.
- Dias, A. M. P. G. et al., 2015. Statistical Analysis of Timber-Concrete Connections – Mechanical Properties. *Computers and Structure* 155, pp. 67-84.
- Du, K., Sun, J. & Xu, W., 2012. *Evaluation of Section and Fiber Integration Point in Fiber Model*. New York, Curran Associates, Inc., pp. 9789-9796.
- Gorst, N. J. S., Williamson, S. J., Pallet, P. F. & Clark, L. A., 2003. *Friction in Temporary Work*, Birmingham: Health and Safety Executive.
- Hassanieh, A., Valipour, H. R., Bradford, M. A. & Sandhaas, C., 2017. Modelling of steel-timber composite connections: Validation of finite element model and parametric study. *Engineering Structures* 138, pp. 35-49.
- Izzi, M., Rinaldin, G. & Fragiaco, M., 2016. *Numerical Modelling of Steel to Timber Joints and Connectors for CLT Structures*. Austria, WTCE.
- Meghlat, E. M., Oudjene, M., Aider, H. A. & Batoz, J. L., 2013. A New Approach to Model Nailed and Screwed Timber Joints using the Finite Element Method. *Construction and Building Materials* 41, pp. 263-269.
- Megson, T. H. G., 2014. *Structural and Stress Analysis*. 3rd ed. Waltham: Elsevier.
- Oudjene, M., Meghlat, E. M., Ait-Aider, H. & Batoz, J. L., 2013. Non-linear Finite Element Modelling of the Structural Behaviour of Screwed Timber-to-Concrete Composite Connections. *Composite Structure* 102, pp. 20-28.
- Oudjene, M. et al., 2018. Finite element modelling of the nonlinear load-slip behaviour of full-scale timber-to-concrete composite T-shaped beams. *Composite Structure*, Volume 196, pp. 117-126.
- Porteous, J. & Kermany, A., 2007. *Structural Timber Design to Eurocode 5*. Victoria: Blackwell Science Ltd.
- Rao, G. A. & Arora, J., 2013. *Strength and Modes of Failure of Adhesive Anchors in Confined Concrete Under Direct Tensile Load*. Toledo, Spanyol, s.n., pp. 1-11.
- Suriani, E., 2012. *Perilaku Sambungan Komposit Kayu-beton Dengan Alat Sambung Sekrup Kunci Terhadap Beban Lateral*. Tesis ed. Yogyakarta: Departemen Teknik Sipil dan Lingkungan UGM. (In Indonesia)
- Tjondro, J. A., Budianto, H. & Aryakusuma, W., 2011. The Flexural Strength and Rigidity of Albasia Nail-Laminated Beam. *Civil Engineering Forum Vol XX/1*, pp. 1211-1218.

[This page is intentionally left blank]